

The twenty-four near-instabilities of Caspar-Klug viruses

François Englert^a, Kasper Peeters^b, Anne Taormina^c

^a*Service de Physique Théorique and The International Solvay Institutes, Université Libre de Bruxelles, Belgium*

^b*Institute for Theoretical Physics, Utrecht University, The Netherlands*

^c*Department of Mathematical Sciences, Durham University, United Kingdom*

(Dated: April 27th, 2008)

Group theoretical arguments combined with normal mode analysis techniques are applied to a coarse-grained approximation of icosahedral viral capsids which incorporates areas of variable flexibility. This highlights a previously overlooked structure of the low-frequency spectrum, namely the existence of a plateau of 24 near zero-modes with universal group theory content.

PACS numbers: 87.15.ad, 87.15.M-, 89.75.Fb

Proteins in a thermal bath exhibit a wide spectrum of dynamical behaviours which can be probed, for instance, by inelastic neutron diffusion (see [1] for a review). In particular, they undergo slow, large-amplitude motions which are now widely believed to be instrumental to their function. These ideas were first tested in [2, 3, 4, 5, 6, 7] where normal mode analysis (NMA) was used to argue that only a few low frequency normal modes of vibration are sufficient to describe, with great accuracy, the conformational changes in a variety of proteins. The method has limitations, as it assumes the existence of a single potential well whose minimum is a given stable conformation of the protein under study, and therefore overlooks the possibility of neighbouring multi-minima of energy reported to exist, in particular at room temperature, in [8, 9, 10]. Furthermore, the harmonic approximation to this single-well potential, which is inherent to NMA, is only valid if the protein's motions are very small, and this does not lend itself to an accurate description of observed conformational changes. Yet, this technique yields dynamical data which are consistent with experimental results on proteins, as observed on case-by-case studies in [11, 12, 13, 14], and is also confirmed by a recent statistical analysis based on a sample of 377 non-redundant protein motions [15]. Although biologically significant low-frequency motions are typically *not* vibrational due to the damping influence of the protein environment, NMA captures the tendency of the biomolecule to change in a few particular directions corresponding to low-frequency normal modes, and thus remains a useful tool when time-dependent methods like molecular dynamics are prohibitive.

The success of NMA in studying protein dynamics has prompted its use in the context of large macromolecular assemblies. The main motivation so far has been to pin down whether several experimentally observed conformations of viral particles could be inferred from one another by arguing that conformational changes occur in directions which maximally overlap with those of a few low-frequency putative normal modes of vibration of the capsid [16, 17, 18, 19]. Viruses are much more complex structures than single proteins, and the biggest challenge remains the choice, within the NMA framework, of a potential which optimally captures the physics of capsid

vibrations whilst taking into account a reduced number of degrees of freedom to enable practical calculations. Many NMA applied to viruses implement variations of the simple Elastic Network Model proposed a decade ago [20], in which the atoms are taken as point masses connected by springs modelling interatomic forces, provided the distance between them is smaller than a given cutoff parameter. Simplified versions include the restriction to C^α -atoms only, the approximation in which each residue is considered as a point mass, or where even larger domains within the constituent coat proteins are treated as rigid blocks [17]. In an effort to optimise the NMA techniques when applied to particles with high symmetry, group theoretical considerations have also been exploited [16, 18]. The basic method is inherited from the classical treatment of small molecule vibrations, which are extensively discussed in the chemistry literature (see for instance [21]). When combined with an Elastic Network approach, it allows for more extensive normal modes calculations of medium size (typically $T = 3$) viral capsids [18] and compares well with results obtained using an Elastic Network-RTB setup [17].

The elastic potential in all analyses above has two major drawbacks: it does not discriminate between strong and weak bonds since it depends on a single spring constant, and it uses the rather crude technique of increasing the distance cutoff to resolve capsid instabilities. Consequently, the frequency spectra have much less structure than one would expect in reality, and in particular fail to reproduce areas of rigidity and flexibility of the capsid satisfactorily. This problem has been addressed in [22], where a bond-cutoff method is implemented. An elastic network whose representatives are $N C^\alpha$ -atoms is set up such that four consecutive C^α -atoms are connected via springs, introducing $3N - 6$ constraints in the system. This backbone modeling provides stability of proteins with a less intricate elastic network than the one obtained via the distance-cutoff method. Further springs with different spring constants are added to model the various types of chemical interactions (disulfide bonds, hydrogen bonds, salt-bridges and van der Waals forces) within each protein. The proposed model reproduces conformational changes better than the conventional distance-cutoff simulations.

In this letter, we propose a reductionist approach to the study of icosahedral viral capsid vibrations within the harmonic approximation, which captures features of the low-frequency spectrum that were hidden in previous analyses, for the reasons highlighted in [22], regarding the use of Tirion’s potential and the distance-cutoff method. We consider Caspar-Klug viral capsids, which are classified according to a triangulation number T [23]. A $T = n$ capsid [28] exhibits $60n$ coat proteins, organised in clusters of twelve pentamers located at the vertices of an icosahedron, and $10(n - 1)$ hexamers at global 3-fold and/or local 6-fold symmetry axes of the icosahedral capsid. In our coarse-graining, these coat proteins are approximated by point masses located at their centres of mass, calculated using the Protein Data Base (PDB). We set up an elastic network whose representatives are these point masses, with all masses normalised to 1. The network topology is determined by data from the VIPER website [24]: two point masses are connected by a spring whenever VIPER provides a value for the association energy of the two corresponding proteins. The spring constants of our model are of the form $\kappa_{mn} = \rho_{mn}\kappa$, with ρ_{mn} the ratio of the association energy of protein pair (m, n) to the largest association energy listed in VIPER, and κ is a free parameter which reflects the lack of confidence in the *absolute* values of association energies published in VIPER. The potential reads,

$$V = \sum_{\substack{m < n \\ m, n=1}}^N \frac{1}{2} \kappa_{mn} (|\vec{r}_m - \vec{r}_n| - |\vec{r}_m^0 - \vec{r}_n^0|)^2, \quad (1)$$

where the vector \vec{r}_m^0 refers to the equilibrium position of protein m , and the vector \vec{r}_m to its position after elastic displacement, all vectors originating from the centre of the capsid. The resulting force (stiffness) matrix thus depends on the parameter κ , and possesses more than the six zero eigenvalues expected from the rotations and translations of the whole capsid whenever the number of constraints imposed by the association energies is smaller than $180n - 6$, where $180n$ is the total number of degrees of freedom for a $T = n$ capsid. Although our model is too crude to account for a realistic flexibility of the viral capsid, and therefore too primitive to get quantitative information on the virus function, it discriminates between strong and weak inter-protein bonds and therefore captures effects of varying flexibility across the capsid. Moreover, it is simple enough to highlight universal aspects of the low-frequency spectrum of normal modes of vibration, inherited from the underlying icosahedral symmetry, and to pin down the influence of the elastic network design on the instability of the capsid.

Our main result, which will be substantiated by group theory arguments below, is the existence, in the low-frequency spectrum of all stable Caspar-Klug capsids, of 24 near-zero normal modes of vibration which always fall in the same set of non-singlet irreducible representations of the icosahedral group (see (4)). The first singlet representation, which is associated with a fully symmet-

ric mode, always appears higher up in the spectrum, in accordance with the expectation that such a motion requires more energy to develop. The presence of 24 near-zero modes in the spectrum of viral capsids is deeply rooted in the fact that the latter exhibit icosahedral symmetry.

To see this, we first approximate a Caspar-Klug $T = n$ capsid by merging the $3n$ proteins per icosahedral face into a single point mass whose equilibrium position is at the centre of the face. These point masses are connected by springs (masses and spring constants normalised to 1) between nearest neighbours, forming a dodecahedral cage with 30 edges, dual to the icosahedron. Such a structure is unstable, since the number of genuine degrees of freedom is $3 \times 20 - 6 = 54$, while there are only 30 constraints. Accordingly, the cage develops 24 non-trivial zero modes. To analyse these instabilities, we compare all possible motions of this dodecahedral cage consistent with icosahedral symmetry, with the dodecahedral motions induced by all possible motions of the 12 vertices of an icosahedron. By induced, we mean that the dual dodecahedron moves in such a way that its vertices are located at the centres of the (deformed) icosahedral faces at all times. Standard group theoretical methods reviewed in [25] are used to calculate the decomposition of the 36-dimensional displacement representation $\Gamma_{\text{ICO}}^{\text{displ},36}$ of the vertices into irreducible representations of the full icosahedral group \mathcal{I}_h , which contains 60 proper rotations and an extra 60 elements obtained by multiplication of the latter by the inversion operation. The result is (see also [26]),

$$\Gamma_{\text{ICO}}^{\text{displ},36} = \Gamma_+^1 + \Gamma_+^3 + 2\Gamma_-^3 + \Gamma_-^{3'} + \Gamma_+^4 + \Gamma_-^4 + 2\Gamma_+^5 + \Gamma_-^5, \quad (2)$$

where the numerical superscripts indicate the dimensionality of the corresponding irreducible representation, while the \pm subscripts refer to different irreducible representations of same dimension [29]. The same group theoretical method yields, for the motion of the dodecahedral cage, the 60-dimensional displacement representation $\Gamma_{\text{DODE}}^{\text{displ},60}$,

$$\Gamma_{\text{DODE}}^{\text{displ},60} = \Gamma_+^1 + \Gamma_+^3 + 2\Gamma_-^3 + \Gamma_-^{3'} + \Gamma_+^4 + \Gamma_-^4 + 2\Gamma_+^5 + \Gamma_-^5 + \Gamma_+^{3'} + \Gamma_-^{3'} + \Gamma_+^4 + \Gamma_-^4 + \Gamma_+^5 + \Gamma_-^5. \quad (3)$$

Although Eq.(2) depends only on icosahedral symmetry and not on actual links between icosahedral vertices, it is useful to visualise an icosahedral cage formed by point masses at its vertices joined by identical springs along its 30 edges. In contradistinction with the dodecahedral cage, the icosahedral cage would have no non-trivial zero-modes, in accordance with the fact that the number of its genuine degrees of freedom $3 \times 12 - 6 = 30$ is equal to the number of its constraints. The spectra of the icosahedral and dodecahedral cages are depicted in Fig.1(a)&(b). As no icosahedral motion leaves the dual dodecahedron fixed, the icosahedral motions induce a 36-dimensional vector space of (infinitesimal) motions of the dual dodecahedron. These include the six global

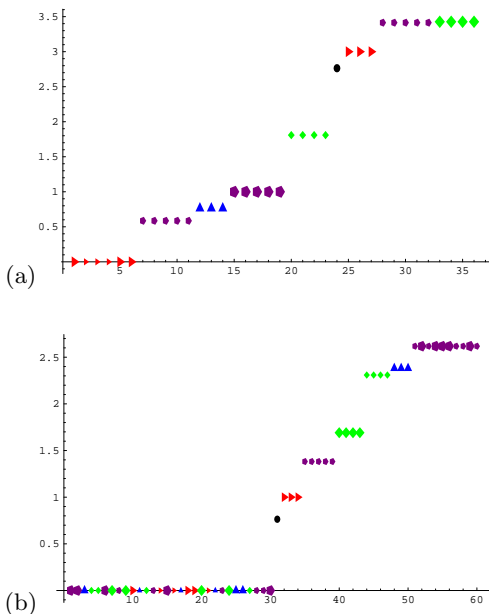


FIG. 1: Frequencies of normal modes of vibration for (a) an icosahedral cage, (b) a dodecahedral cage. The modes \triangleright resp. \triangle belong to 3-dimensional irreducible representations Γ_{\pm}^3 resp. $\Gamma_{\pm}^{3'}$ of the icosahedral group. The diamond (resp. pentagon) modes belong to 4 (resp. 5)-dimensional irreducible representations. Small (large) symbols refer to even (odd) parity. The x-axis labels the normal modes while the y-axis gives the wave numbers up to an overall normalisation.

zero-modes $\Gamma_+^3 + \Gamma_-^3$ which are identical in both systems (as well as the global dilation vibrational mode Γ_+^1). All icosahedral normal modes of vibration pertaining to an irreducible representation of \mathcal{I}_h in $\Gamma_{\text{ICO}}^{\text{displ},36}$ must be linear combination of dodecahedral normal modes belonging to the same irreducible representation. Hence, provided that the vibrational modes of the icosahedron have non-vanishing components in the vibrational modes of finite frequency of the dodecahedron, as is true by inspection, the set of representations in (3) which are not contained in (2) describe the non-trivial zero-modes of the dodecahedron. It follows that a capsid whose proteins would be modelled by twenty point masses located at the centre of each face of an icosahedron, and with thirty springs organised in a network modelled at equilibrium by a dodecahedron, develops 24 zero-modes of vibration which are organised in the following irreducible representations of the icosahedral group,

$$\Gamma_+^{3'} + \Gamma_-^{3'} + \Gamma_+^4 + \Gamma_-^4 + \Gamma_+^5 + \Gamma_-^5. \quad (4)$$

Note that the zero-modes belonging to the $\Gamma_+^{3'}$ representation appear in (3) but have no counterpart in (2). Hence they must induce no motion when mapped back to an icosahedral system, that is, the sum of the displacements of any 5 vertices defining a dodecahedral face must be zero. This is indeed the case as illustrated in Fig. 2, where the icosahedral system may be thought of as constructed

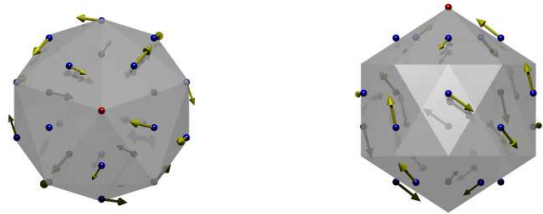


FIG. 2: Top and side views of the normal modes of a dodecahedral system belonging to the irreducible representation $\Gamma^{3'}$ of the icosahedral group \mathcal{I} .

from the centre-of-mass positions of the dodecahedron vertices of each pentagon face. The stabilisation of such a capsid requires the introduction of at least 24 further springs in a manner that respects the icosahedral symmetry. The magnitudes of the spring constants determine how much the zero-modes are lifted from zero, and shape the structure of the created low-frequency plateau.

Despite its simplicity, the approximation just described catches an essential feature of the Caspar-Klug viruses, namely the 24 low-energy plateau with group content (4). Indeed, consider again a $T = n$ capsid with $3n$ proteins per icosahedral face but now treat them, in accordance with our introductory discussions, as $3n$ point masses located at the corresponding protein's centre of mass calculated from the PDB files. We link them by springs according to the association energies listed in VIPER [30]. Neglecting first the links between different faces, we would expect a number of capsid zero-modes, $N_0 = (9n - 3k) \cdot 20 = 60(3n - k)$. Here the $9n$ degrees of freedom within a face are constrained only by $3k$ links, k integer, as a consequence of the global 3-fold symmetry of the icosahedron whose axis passes through the centre of the icosahedral face. A stable capsid is characterised by a force matrix having exactly six zero-modes, so that in principle, one needs to introduce at least $60(3n - k) - 6$ independent constraints (i.e. bonds) to stabilise the whole capsid. How these must be chosen in a 3-dimensional context is a mathematical question which requires further investigation. It is however interesting to note that the VIPER website gives association energies for some inter-face proteins, which correspond to ‘[icosahedron] edge-crossing’ bonds. By symmetry, these come as multiples of 30 or 60 when considering the capsid as a whole. We thus expect that, keeping the $2(3n - k) - 1$ edge-crossing bonds per edge with the largest association energies, would yield a capsid with 24 non-trivial zero modes. In all stable capsids we studied [27], this indeed happens, and adding extra edge-crossing bonds lifts the 24 zero-modes appearing in (4) to a low-frequency plateau. Our earlier approximation thus simply amounts to replacing $3n - k$ by unity in the above analysis.

We now illustrate our considerations with two examples. The VIPER data for the $T = 3$ Rice Yellow Mottle Virus (PDB: 1f2n) is sufficient to stabilise the capsid. It is reproduced schematically in Fig. 3 [31] together

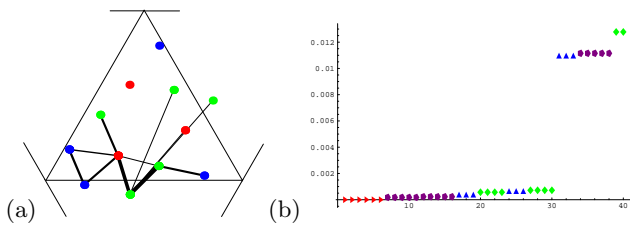


FIG. 3: (a) Bond structure of RYMV as given in VIPER, (b) Its forty lowest frequency modes showing a plateau of 24 near-zero modes.

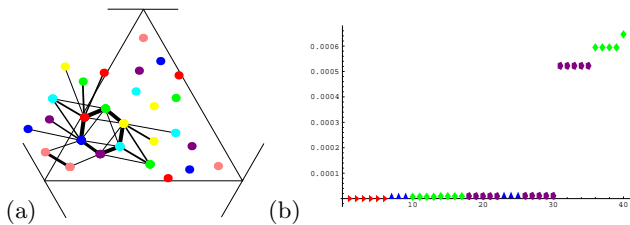


FIG. 4: (a) Bond structure of HK97 as given in VIPER, (b) Its forty lowest frequency modes showing a plateau of 24 near-zero-modes with the representation content of (4).

with the 40 lowest-frequency normal modes of vibration.

The capsids in our examples are not invariant under inversion, hence the symmetry group is \mathcal{I} , and the irreducible representations are all of type ‘+’. Discarding the two weakest bonds (which are both edge-crossing) leads to $k = 4$ and 9 edge-crossing bonds per edge. In agreement with $2(3n - k) - 1 = 9$ we then observe 24 non-trivial zero modes. Restoring the weak long-range arms which stretch from the (green) C-chains has the crucial effect of lifting the 24 zero modes to produce a low-frequency plateau. The $T = 7\ell$ Hong-Kong 97 bacteriophage (PDB: 2fte) has a stable capsid too. Keeping all but the six weakest bonds [32] leads to $k = 12$ and 17 edge-crossing bonds per edge, in accordance with $2(3n - k) - 1 = 17$, so that there are 24 non-trivial zero modes. The weak bonds serve to lift these zero modes, and the spectrum indeed exhibits again a very low-frequency plateau of 24 modes (see Fig. 4). A variety of other capsids with similar spectral signatures are presented in [27]. Although there exist several viruses NMA in the recent literature, it is difficult at this stage to make meaningful comparisons, given the limitations mentioned in our introductory statement. Still, the first non-zero mode (a singlet of \mathcal{I}) in the spectrum of HK97, as calculated in [19] using an all-atom simulation with a 7.3\AA cutoff, appears at mode 31 and is therefore compatible with our qualitative arguments on the number of low-frequency modes.

-
- [1] J. C. Smith, *Structure and Dynamics of Biomolecules* (Oxford University Press, 2000), pp. 161–180.
- [2] J. A. McCammon, B. R. Gelin, M. Karplus, and P. Wolynes, *Nature* p. 325 (1976).
- [3] T. Noguti and N. Go, *Nature* **296**, 776 (1982).
- [4] B. R. Brooks and M. Karplus, *Proc. Nat. Acad. Sci.* **80**, 6571 (1983).
- [5] N. Go, T. Noguti, and T. Nishikawa, *Proc. Nat. Acad. Sci.* **80**, 3696 (1983).
- [6] M. Levitt, C. Sander, and P. Stern, *Int. J. Quant. Chem.* **10**, 181 (1983).
- [7] R. Harrison, *Biopolymers* **23**, 2943 (1984).
- [8] R. Elber and M. Karplus, *Science* **235**, 318 (1987).
- [9] H. Frauenfelder, F. Parak, and R. D. Young, *Annu. Rev. Biophys. Biophys. Chem.* **17**, 451 (1988).
- [10] M. K. Hong et al., *Biophys. J.* **58**, 429 (1990).
- [11] B. R. Brooks and M. Karplus, *Proc. Nat. Acad. Sci.* **82**, 4995 (1985).
- [12] J. F. Gibrat and N. Go, *Proteins* **8**, 258 (1990).
- [13] O. Marques and Y. H. Sanejouand, *Proteins* **23**, 557 (1995).
- [14] L. Mouawad and D. Perahia, *J. Mol. Biol.* **258**, 393 (1996).
- [15] V. Alexandrov et al., *Protein Sci.* **14**, 633 (2004).
- [16] T. Simonson and D. Perahia, *Biophys. J.* **61**, 427 (1992).
- [17] F. Tama and C. L. Brooks, *J. Mol. Biol.* **318**, 733 (2002).
- [18] H. W. T. v. Vlijmen and M. Karplus, *J. Mol. Biol.* **350**, 528 (2005).
- [19] A. Rader, D. Vlad, and I. Bahar, *Structure* **13**, 413 (2005).
- [20] M. M. Tirion, *Phys. Rev. Lett.* **77**, 1905 (1996).
- [21] F. A. Cotton, *Chemical Applications of Group Theory* (Wiley, New York, 1990).
- [22] J. I. Jeong, Y. Jang, and M. K. Kim, *J. Mol. Graphics and Modelling* **24**, 296 (2006); *Int. J. Control, Automation and Systems* **4**, 382 (2006); *Nucl. Acids Res.* **34**, W57 (2006).
- [23] D. Caspar and A. Klug, *Cold Spring Harbor Sympos. Quant. Biol.* **27**, 1 (1962).
- [24] C. Shepherd, I. Borelli, G. Lander, P. Natarajan, V. Sidavanahalli, C. Bajaj, J. Johnson, C. I. Brooks, and V. Reddy, *Nucl. Acids Res.* **34**, D386 (2006).
- [25] K. Peeters and A. Taormina, in *Proceedings of the Second Mathematical Virology Workshop, Edinburgh, 6-10 August 2007* (2008), arXiv:0802.2620.
- [26] M. Widom, J. Lidmar, and D. R. Nelson, *Phys. Rev.* **E76**, 031911 (2007), arXiv:0706.4291.
- [27] K. Peeters and A. Taormina (2008), in preparation.
- [28] $n = h^2 + hk + k^2$ for h and k integer and relatively prime.
- [29] If the subgroup \mathcal{I} of 60 proper rotations is used instead, \pm representations are indistinguishable.
- [30] In [25], the radial projections of these point mass coordinates onto icosahedron faces were used, blurring stability issues.
- [31] There are actually 11 bonds in Fig. 3, but 3 of them are superimposed (2 linking green C-chains, and one linking a C- and a B-chain (red)). The total number of bonds is obtained from the figure using the global 2-, 3- and 5-fold symmetries of the capsid.
- [32] Only one of them is edge-crossing in Fig. 4.